Effects of size and spacing of uniformly distributed pearlite particles on fatigue crack growth behavior of ferrite–pearlite steels

Mohammad Sukri Mustapa [a,b], Yoshiharu Mutoh [a,*]

[a] *Department of Material Science, Nagaoka University of Technology, 1603-1 Kamitomioka, Nagaoka, Niigata 940-2188, Japan*
[b] *Faculty of Mechanical and Manufacturing, Tun Hussein Onn University of Malaysia (UTHM), Parit Raja, Batu Pahat, 86400 Johor, Malaysia*

ABSTRACT

Fatigue crack growth tests of three ferrite–pearlite steels with different size and spacing of pearlite particles, which were uniformly distributed in the ferrite matrix, were carried out to investigate the effect of microstructure on fatigue crack growth behavior in the Paris regime. The fatigue crack growth rates for the three materials did not coincide with each other, even when the crack growth curves were arranged by the effective stress intensity factor range. From in situ observations, crack tip stress shielding phenomena, such as interlocking and branching, were found on the crack wake, which enhanced fatigue crack growth resistance. A small size and spacing of pearlite particle seemed to induce small but frequent crack deflections, which resulted in crack closure phenomena. On the other hand, the large size of the pearlite particle seemed to induce stress shielding phenomena and, thus, contribute to high crack growth resistance, which was the main reason for the higher fatigue crack growth resistance of the large size and spacing of pearlite particles compared to the small size of pearlite particles.

1. Introduction

There is a large number of research regarding the effect of microstructure on fatigue crack growth behavior in the near threshold region [1–10], for example, large grains are known to contribute to a high threshold value [3,11–13]. On the other hand, research regarding the effect of microstructure on fatigue crack growth behavior in the so-called Paris regime have rarely been reported. If the effect of microstructure on fatigue crack growth resistance in the Paris regime could be made clear in detail, fatigue crack growth resistance could be improved by controlling the microstructure. Although only limited information is available on the detailed influence of microstructure on fatigue crack growth resistance in the Paris regime, some important works on fatigue crack growth behavior of two phase steels have been reported [5,7,14–24].

In previous research [5,10], fatigue crack growth tests of ferrite–pearlite steels with three different pearlite phase morphologies were carried out in the Paris regime to investigate the effect of pearlite morphology. The three different pearlite phase morphologies were uniformly distributed pearlite particles in a ferrite matrix (Steel D), layered pearlite bands in a ferrite matrix (Steel B) and a coarse networked pearlite phase with an encapsulated

ferrite phase (Steel N). It was found that a microstructure with uniformly distributed pearlite particles (Steel D) showed higher fatigue crack growth resistance compared to those with layered pearlite bands (Steel B) and with a coarse networked pearlite phase (Steel N). It was also found from the in situ observations and fracture mechanics discussion that the crack path of Steel D was frequently deflected on the micro scale due to distributed pearlite particles, which induced interlocking between crack surfaces and, thus, crack tip stress shielding. It was concluded that this significant crack tip stress shielding phenomena in Steel D contributed to the higher fatigue crack growth resistance compared to the other microstructures. However, the optimal size and spacing of pearlite particle in Steel D are still unclear. Once the detailed effects of pearlite particle size and spacing on fatigue crack growth behavior and resistance in microstructures with uniformly distributed pearlite particles in a ferrite matrix is clarified, fatigue crack growth resistance can be improved.

In the present study, uniformly distributed pearlite particle microstructure steels (steel D) with different spacing and size of pearlite particles were prepared for further investigation of the effect of pearlite particle size and spacing on fatigue crack growth behavior in the Paris regime. ΔK-constant fatigue crack growth tests were carried out inside a scanning electron microscope chamber equipped with a servo-hydraulic fatigue test machine. During the tests, in situ crack path observations were carried out to identify the crack tip stress shielding phenomena, such as interlocking and crack branching. From the results, the influence of pearlite particle

* Corresponding author. Tel.: +81 258 47 9735; fax: +81 258 47 9770.
E-mail address: mutoh@mech.nagaokaut.ac.jp (Y. Mutoh).

Table 1
Chemical composition of the steel used (mass%).

C	Si	Mn	P	S
0.22	0.32	1.08	0.003	0.001

Table 2
Microstructural characteristics of the three materials used.

	FP1	FP2	FP3
Ferrite grain size (μm)	50	10	65
Pearlite volume fraction (%)	50	50	30
Spacing of pearlite particle (μm)	70	12	80
Size of pearlite particle (μm)	70	5	50
Vickers hardness Ferrite (50 g)	112	132	125
Vickers hardness Pearlite (50 g)	201	205	214

Table 3
Mechanical properties of the three materials used.

	FP1	FP2	FP3
Yield strength (0.2%) (MPa)	236	310	224
Tensile strength (MPa)	475	492	486
Elongation (%)	38	38	37

spacing and size on fatigue crack growth resistance was determined in detail.

2. Experimental procedures

2.1. Materials

The material used in this study was a ferrite–pearlite steel with uniformly distributed pearlite particles in a ferrite matrix, the chemical composition of which is shown in Table 1. Three microstructures with different size and spacing of pearlite particle were prepared from the same starting steel by thermo-mechanical control processing (Fig. 1). The microstructural characteristics and mechanical properties of the three materials are also shown in Tables 2 and 3, respectively, where the materials FP1 and FP2 have the same pearlite volume fraction but different particle size and spacing; FP2 has a finer microstructure compared to FP1. The materials FP1 and FP3 have different volume fractions of the pearlite phase but similar pearlite particle size; FP3 has a lower volume fraction of the pearlite phase compared to FP1.

2.2. Fatigue crack growth test

Single edge cracked plate tension type specimens with a width of 5 mm and a thickness of 1.5 mm were used for fatigue crack growth tests (Fig. 2). A notch with a width of 0.1 mm and a depth of 0.5 mm was introduced by electric discharge machining (EDM) at the edge of the specimen as a starter for fatigue crack growth. Prior to the fatigue crack growth test, the specimen surface
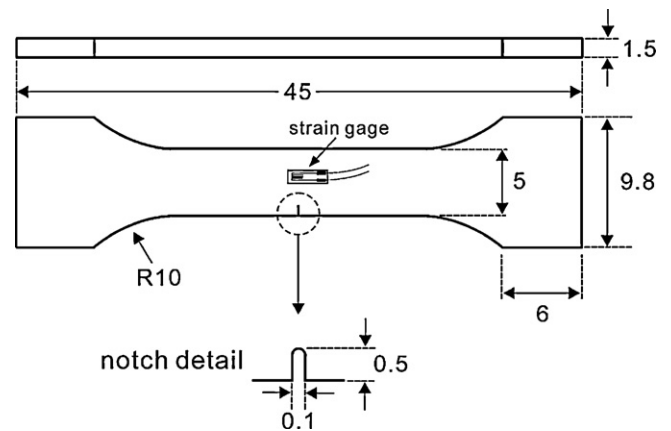
Fig. 2. SECT specimen geometry for the fatigue crack growth test (units in mm).

was etched by a 3% nital solution for in situ crack path observation.

Fatigue tests were performed inside a scanning electron microscope (SEM) chamber equipped with a servo-hydraulic testing machine. The SEM was also equipped with video recording and image processing systems, which were connected to a personal computer. During the tests, in situ SEM observations of crack growth behavior were carried out in detail. The tests were conducted using a sinusoidal form of loading with a stress ratio of 0.1 and a frequency of 20 Hz.

The ΔK-constant fatigue crack growth tests at $\Delta K = 12\,\mathrm{MPa}\sqrt{\mathrm{m}}$ in the Paris regime were carried out. The detailed test procedure is as follows. Once a fatigue crack starts to propagate from a notch under a constant stress amplitude, the test is continued until the ΔK value reaches the target ΔK value of $12\,\mathrm{MPa}\sqrt{\mathrm{m}}$. Then, the ΔK value is kept constant by reducing the load to less than 3% of the previous load. At this stage, all photographs of the fatigue crack path were taken at the maximum load.

Crack closure behavior was monitored by using the unloading elastic compliance method [25] with a strain gauge attached in front of the crack tip, as shown in Fig. 2. The effective stress intensity factor range, ΔK_{eff}, was evaluated based on the crack closure measurement as:

$$\Delta K_{eff} = K_{\max} - K_{cl} \tag{1}$$

where K_{max} is the maximum stress intensity factor and K the stress intensity factor at the crack closure stress. The crack growth rate was determined from the crack length vs. number of cycles curves by using the secant method (ASTM E647). The stress intensity factor, K, for the present specimen was calculated according to the following equation [26]:

$$K = \sigma\sqrt{\pi a}F_I(\alpha), \quad \alpha = \frac{a}{W} \tag{2}$$

$$F_I(\alpha) = 1.12 - 0.231\alpha + 10.55\alpha^2 - 21.72\alpha^3 + 30.39\alpha^4 \tag{3}$$
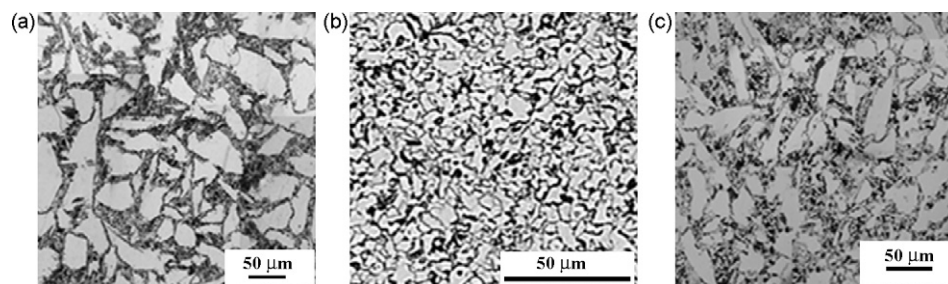
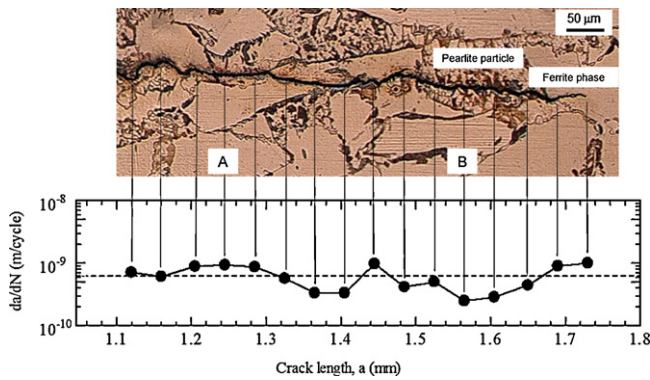**Fig. 1.** Microstructures of the three materials used (Light etching phase, ferrite; dark, pearlite).
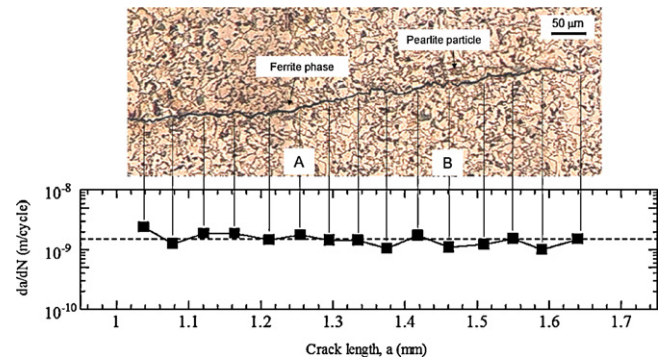
Fig. 3. Crack path and crack growth rates for FP1.

Fig. 5. Crack path and crack growth rates for FP2.

where σ is the stress, a the crack length, W the width of the gauge part of the specimen and F_I is a geometrical correction factor.

3. Results and discussion

3.1. In situ observations of fatigue crack growth behavior

Fig. 3 shows the fatigue crack path for FP1 during the ΔK-constant fatigue crack growth test. In the figure, the corresponding fatigue crack growth rates are also indicated. As seen from the figure, the crack passed through the pearlite particles. Symbol A indicates a region with higher crack growth rates, where the crack propagates in a flat manner, as shown in Fig. 4(a). On the other hand, symbol B indicates a region with lower crack growth rates, where the crack propagates in a zigzag manner through a pearlite particle, as shown in Fig. 4(b), which reveals the interlocking of crack surfaces ($\triangle$) and the branching of crack ($\blacktriangle$).

Fig. 5 shows the fatigue crack path and crack growth rates for FP2. As seen from the figure, the crack seemed to frequently deflect at pearlite particles and the variation of the growth rate was less than that for FP1. Region A, with higher fatigue crack growth rates, displays a rather smooth flat crack path, as shown in Fig. 6(a). On the other hand, region B, with lower fatigue crack growth rates, shows a tortuous crack path, which results in crack tip stress shielding phenomena, such as interlocking and branching, as shown in Fig. 6(b). However, the stress shielding phenomena of FP2 seemed to be insignificant compared to that of FP1.

Fig. 7 shows the fatigue crack path and crack growth rates for FP3. As seen from the figure, larger crack deflections were observed compared to FP2. The higher crack growth rate region, region A, displays a flat crack path, while the lower crack growth rate region, region B, displays a tortuous crack path with interlocking and branching, as shown in Fig. 8(a) and (b), respectively.

Based on these in situ crack path observations, it seemed that crack tip stress shielding phenomena, such as interlocking and branching, were more significant and more frequently observed in FP1, while they were observed less frequently in FP3 and even less in FP2. Both interlocking and branching contribute to the stress shielding effect. However, the quantitative influence of these phenomena has not yet been clarified. In the present study, the combined total contribution to the stress shielding effect without any distinction of each individual influence, is considered.

3.2. Effect of crack closure phenomena

Fig. 9 shows a comparison of the average crack growth rates of FP1, FP2 and FP3. As seen from the figure, the fatigue crack growth resistance of FP1 was the highest, whereas that of FP3 was the lowest.

The first step towards understanding the reason for the difference in fatigue crack growth resistance of the three microstructures was an investigation of the effect of crack closure. From the crack closure load measurements using the unloading elastic compliance method, the relationships between fatigue crack growth rate and the crack opening ratio for the three materials are shown in Fig. 10, where the crack opening ratio is given as:

$$U = \frac{K_{\max} - K_{cl}}{K_{\max} - K_{\min}} = \frac{\Delta K_{eff}}{\Delta K} \tag{4}$$

As seen in the figure, crack closure was much more significant in FP1 and FP2 and less significant in FP3. The fatigue crack growth curves for the three materials were arranged by using ΔK_{eff}, as shown in Fig. 11. It was found from this figure that the $(da/dN) - \Delta K_{eff}$ curves for FP1, FP2 and FP3 did not coincide with each other.

This suggests that some mechanisms other than crack closure influence fatigue crack growth resistance. Korda et al. [5] clearly determined that crack tip stress shielding due to interlocking and
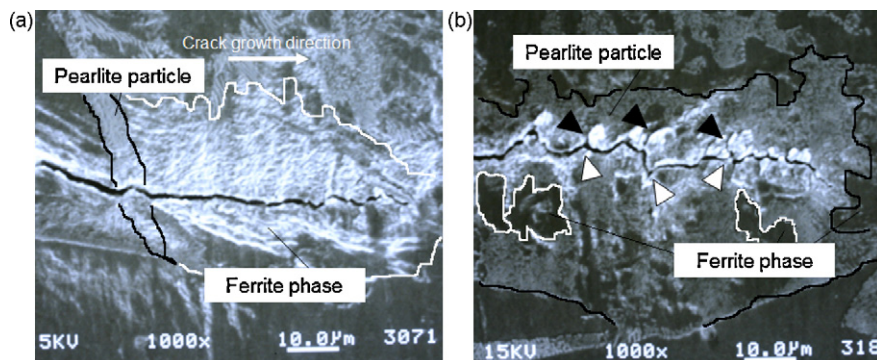

Fig. 4. Crack path at higher magnification for FP1: (a) crack path at A and (b) crack path at B. ($\blacktriangle$: branching; $\triangle$: interlocking)
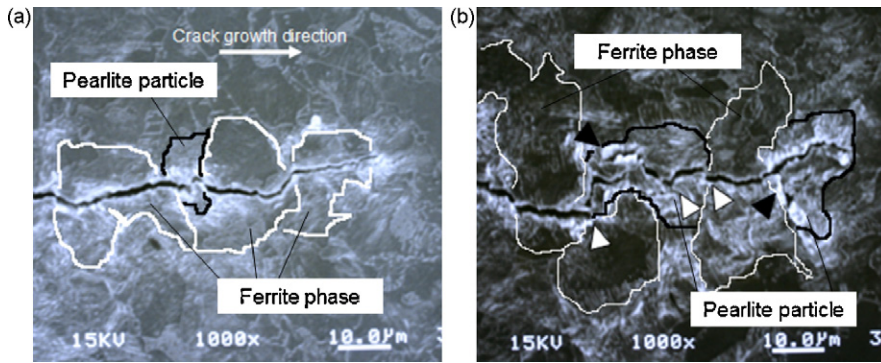
Fig. 6. Crack path at higher magnification for FP2: (a) crack path at A and (b) crack path at B. (▲: branching; △: interlocking)
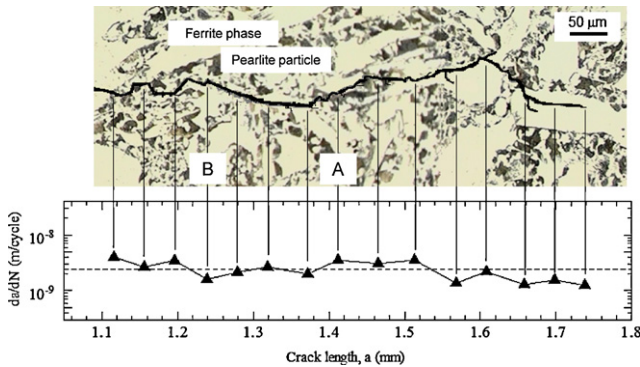

Fig. 7. Crack path and crack growth rates for FP3.

Fig. 9. Comparison of crack growth rates for the three materials investigated.

crack branching was the corresponding mechanism. As shown in Figs. 4, 6 and 8, interlocking and crack branching elements were often observed on the crack wake for all three materials, FP1, FP2 and FP3.

3.3. Effect of crack tip stress shielding

To investigate the effect of crack tip stress shielding on fatigue crack growth resistance, the effective crack tip stress intensity factor range, $\Delta K_{eff,tip}(=K_{tip} - K_{cl})$, was evaluated according to the method indicated in previous papers [5,10], where both crack closure and crack tip stress shielding effects were taken into consideration, as seen in Fig. 12.

From the results, the fatigue crack growth curves for FP1, FP2 and FP3 were rearranged by using $\Delta K_{eff,tip}$, as shown in Fig. 11. The resultant fatigue crack growth curves for the three materials were merged into one curve, which suggested that $\Delta K_{eff,tip}$ would
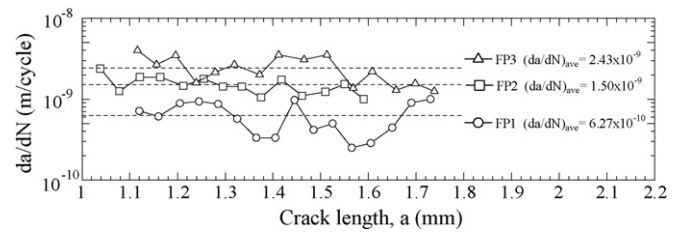
be the intrinsic controlling fracture mechanics parameter for the materials with crack tip stress shielding phenomena during fatigue crack growth. At the same time, it was found that the effect of crack tip stress shielding was the most significant in FP1 with the largest pearlite particles.

3.4. Effects of pearlite particle size and spacing

From the foregoing results, a comparison of the three materials in terms of interlocking/branching, crack deflection, crack closure and stress shielding phenomena is summarized in Table 4. As seen from the table, FP2 showed significant crack closure, where the degree of crack deflection was small but was frequently observed compared to the other two materials. These small but frequent crack deflections resulted from small particle size and spacing. Therefore, the frequent crack deflection might be the reason for the significant crack closure in FP2. FP1 also showed significant crack closure. The crack path in the pearlite particle in FP1 seemed more tortuous compared to that in FP3, as seen in Fig. 4(b) and Fig. 8(b). The cracks passed through the large pearlite particles in FP1 and FP3 and the most significant crack tip stress shielding effect was found in FP1, where interlocking of crack surfaces and crack branching
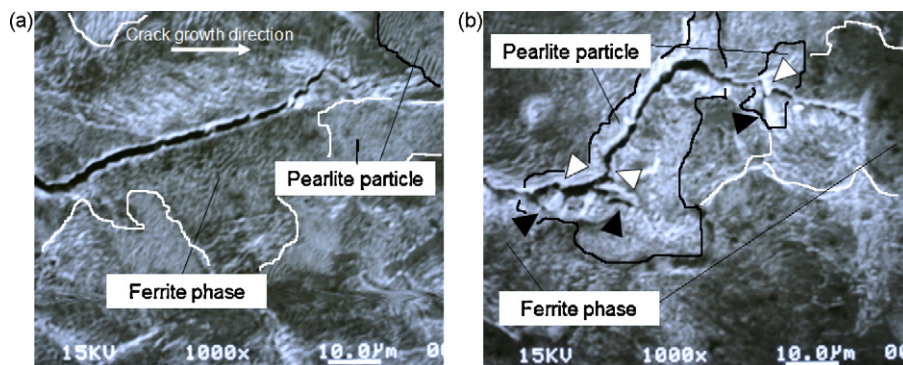

Fig. 8. Crack path at higher magnification for FP3: (a) crack path at A and (b) crack path at B. (▲: branching; △: interlocking)
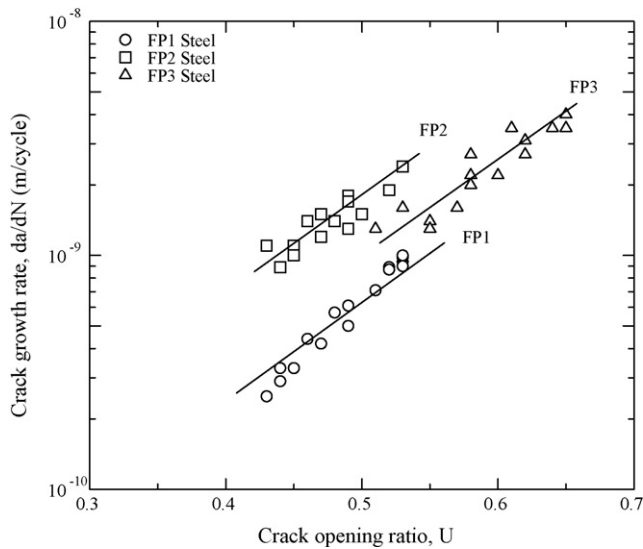
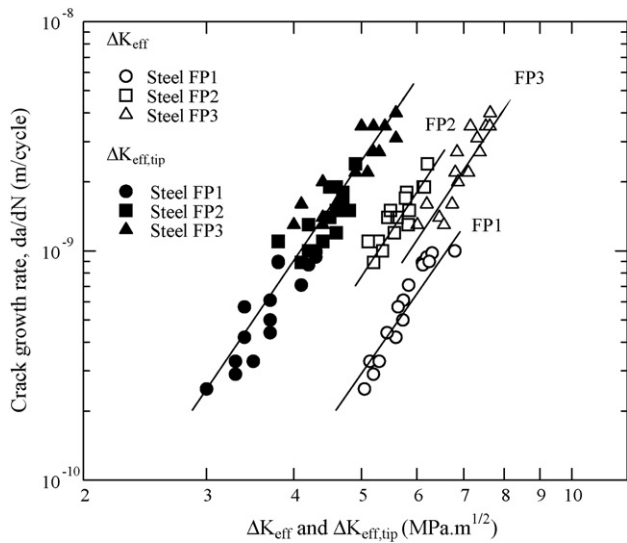**Fig. 10.** Relationship between crack growth rate and crack opening ratio.

Fig. 11. Relationships between crack growth rate, da/dN and stress intensity factor ranges ΔK_{eff} and $\Delta K_{eff,tip}$.
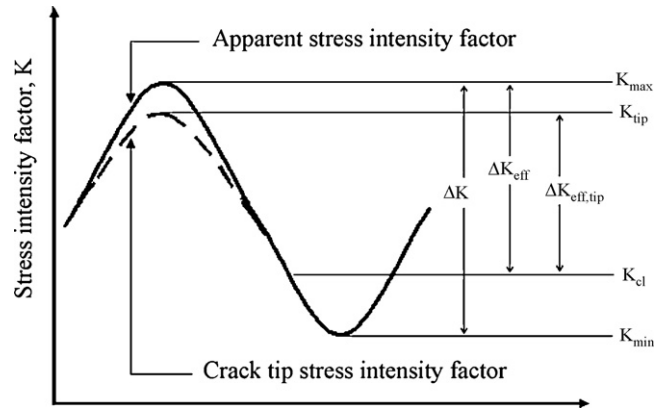

Fig. 12. Definition of the crack tip effective stress intensity factor range $\Delta K_{eff,tip}$.

were more often observed compared to the other two materials. The frequent interlocking and crack branching is the reason for the significant crack tip stress shielding effect.

Although FP3 indicated similar crack growth behavior to FP1, it showed less crack tip stress shielding and lower crack growth resistance compared to FP1. The volume fraction of pearlite in FP3 was low compared to FP1 and the size and spacing of pearlite particle in FP3 were smaller and larger compared to FP1, respectively. These microstructural differences may be the reason for the difference in the stress shielding effect between FP1 and FP3.

The cyclic plastic zone size at $\Delta K = 12$ MPa$\sqrt{m}$ is of the order of 150 μm (100–190 μm) for the present materials. The pearlite particle size of FP2 seems to be small enough compared to the plastic zone size for the crack to deflect at the particles. On the other hand, the pearlite particle sizes of FP1 and FP3 seem to be large enough compared to the plastic zone size, so the cracks tend to pass through the particles more than deflect at the particle.

From the foregoing discussion, assuming that the crack tip stress shielding effect is proportional to pearlite particle size, the shielding stress intensity factor, K_s, can be estimated as follows. From Fig. 11, the values of ΔK_{eff} and $\Delta K_{eff,tip}$ at 10^{-9} m/cycle for the three materials are listed in Table 5. Experimental values of the shielding stress intensity factor, K_s (=$\Delta K_{eff} - \Delta K_{eff,tip}$), are also indicated in the table. Based on the average pearlite particle size and spacing shown in Table 2, the length of the pearlite phase per length of 140 μm were calculated and, are indicated in Table 5. The ratios of pearlite phase length normalized by the pearlite phase length of FP1 are also shown in the table. Using these ratios, the K_s values of FP2 and FP3 which are listed in Table 5 were estimated. As seen in the table, the estimated K_s value of FP3 was in good agreement with

Table 4
FCG behavior of the three materials.

	Particle spacing	Particle size	Crack deflection	Closure	Interlocking/branching	Stress shielding
FP1	Medium (70 μm)	Large (70 μm)	Medium	More	More	More
FP2	Small (12 μm)	Small (5 μm)	Small/frequent	More	Less	Less
FP3	Large (80 μm)	Medium (50 μm)	Large	Less	Medium	Medium

Table 5
Estimation of shielding stress intensity factor, K_s.

	FP1	FP2	FP3
ΔK_{eff} at 10^{-9} m/cycle	6.5	5.2	6.0
$\Delta K_{eff,tip}$ at 10^{-9} m/cycle	4.1	4.1	4.1
K_s (=$\Delta K_{eff} - \Delta K_{eff,tip}$)	2.4	1.1	1.9
Cumulative pearlite phase fraction per length of 140 μm	70	40	55
Ratio of the fraction	1	0.57	0.79
Estimate of K_s value by using pearlite phase fraction ratio	2.4	1.4	1.9

the experimental K_s value, while the estimated K_s value of FP2 was higher than the experimental value. This lower K_s value resulted from the deflection of the crack path at pearlite particles.

From the foregoing discussion, in microstructure with uniformly distributed pearlite particles in a ferrite matrix, a higher volume fraction of pearlite and larger pearlite particle size might be beneficial for enhancing crack tip stress shielding and, thus, fatigue crack growth resistance.

4. Conclusions

From the results of (K-constant fatigue crack growth tests in the Paris regime, the roles of crack closure and crack tip stress shielding on fatigue crack growth resistance for ferrite–pearlite steels with uniformly distributed pearlite particles were investigated. The effects of the spacing and size of pearlite particle on crack closure and crack tip stress shielding were also discussed based on detailed in situ SEM observation of fatigue crack growth behavior. The main conclusions obtained are summarized as follows:

(1) Even in the Paris regime, fatigue crack growth rates for the three materials with different pearlite particle sizes and spacings did not coincide with each other. The material with large spacing and size of pearlite particle showed higher fatigue crack growth resistance.
(2) Small spacing and size of pearlite particles induced small but frequent crack path deflection, which contributed to crack closure due to the roughness induced crack closure mechanism.
(3) A higher volume fraction of pearlite and large size of pearlite particle would be beneficial for enhancing crack tip stress shielding and, thus, fatigue crack growth resistance.
(4) The fatigue crack growth curves for the three materials coincided with each other when both crack closure and crack tip stress shielding were taken into consideration, where the effective crack tip stress intensity factor range, $\Delta K_{eff,tip}$, was the parameter for controlling the fatigue crack growth rate.

Acknowledgements

References

[1] K. Minakawa, Y. Matsuo, A.J. McEvily, Metallurgical Transactions A: Physical Metallurgy and Materials Science 13A (1982) 439–445.
[2] K. Minakawa, A.J. McEvilv, Strength of Metals and Alloys. Proceedings of the 5th International Conference, 27–31 August, Pergamon, Aachen, West Germany, 1979, pp. 1145–1150.
[3] Y. Mutoh, V.M. Radhakrishnan, Transactions of the ASME: Journal of Engineering Materials and Technology 108 (1986) 174–178.
[4] J.L. Horng, M.E. Fine, Materials Science and Engineering 67 (1984) 185–195.
[5] A.A. Korda, Y. Miyashita, Y. Mutoh, T. Sadasue, International Journal of Fatigue 29 (2007) 1140–1148.
[6] D. Chen, Z. Wang, X. Jiang, S. Ai, C. Shi, Steel Research 59 (1988) 319–322.
[7] V.B. Dutta, S. Suresh, R.O. Ritchie, Metallurgical Transactions A: Physical Metallurgy and Materials Science 15A (1984) 1193–1207.
[8] M.T. Yu, T.H. Topper, International Journal of Fatigue 11 (1989) 335–340.
[9] W. Zhongguang, W. Guonan, K. Wei, H. Haicai, Materials Science and Engineering 91 (1987) 439–444.
[10] Y. Mutoh, A.A. Korda, Y. Miyashita, T. Sadasue, Materials Science and Engineering A 468–470 (2007) 114–119.
[11] J. Masounave, J.P. Bailon, Scripta Metallurgica 10 (1976) 165–170.
[12] S. Taira, K. Tanaka, M. Hoshina, ASTM Special Technical Publication 675, 1979, pp. 135–173.
[13] R. Pippan, Materials Science and Engineering A: Structural Materials: Properties, Microstructure and Processing A138 (1991) 1–13.
[14] A.A. Korda, Y. Mutoh, Y. Miyashita, T. Sadasue, Materials Science and Engineering A 428 (2006) 262–269.
[15] A.A. Korda, Y. Mutoh, Y. Miyashita, T. Sadasue, S.L. Mannan, Scripta Materialia 54 (2006) 1835–1840.
[16] A.J. McEvily, K. Minakawa, Scripta Metallurgica 18 (1984) 71–76.
[17] J.A. Wasynczuk, R.O. Ritchie, G. Thomas, Materials Science and Engineering 62 (1984) 79–92.
[18] S. Suresh, Metallurgical Transactions A: Physical Metallurgy and Materials Science 14A (1983) 2375–2385.
[19] H. Suzuki, A.J. McEvily, Metallurgical Transactions A: Physical Metallurgy and Materials Science 10A (1979) 475–481.
[20] A. Bag, K.K. Ray, E.S. Dwarakadasa, Metallurgical and Materials Transactions A: Physical Metallurgy and Materials Science 32 (2001) 2207–2217.
[21] J.R. Hwang, K.P. Peng, C.C. Wang, Journal of Materials Science Letters 15 (1996) 192–196.
[22] J.K. Shang, J.-L. Tzou, R.O. Ritchie, Metallurgical Transactions A: Physical Metallurgy and Materials Science 18A (1987) 1613–1627.
[23] J.L. Tzou, R.O. Ritchie, Scripta Metallurgica 19 (1985) 751–755.
[24] D.L. Chen, Z.G. Wang, X.X. Jiang, S.H. Al, C.H. Shih, Materials Science and Engineering A: Structural Materials: Properties, Microstructure and Processing A108 (1989) 141–151.
[25] M. Kikukawa, M. Jono, K. Tanaka, M. Takatani, Journal of the Society of Materials Science Japan 25 (1976) 899–903.
[26] W.F. Brown Jr., J.E. Srawley, ASTM Special Technical Publication 410 1966, American Society for Testing Materials, Philadelphia, 1996, p. 12.